Effective Geometric Size and Bond-Loss Effect in Nano-elasticity of GaN Nanowires

R.J. Wang , C.Y. Wang , Y.T. Feng

PII: S0020-7403(17)30722-1
DOI: 10.1016/j.ijmecsci.2017.06.026
Reference: MS 3755

To appear in: *International Journal of Mechanical Sciences*

Received date: 22 March 2017
Revised date: 4 June 2017
Accepted date: 16 June 2017

Please cite this article as: R.J. Wang , C.Y. Wang , Y.T. Feng , Effective Geometric Size and Bond-Loss Effect in Nano-elasticity of GaN Nanowires, *International Journal of Mechanical Sciences* (2017), doi: 10.1016/j.ijmecsci.2017.06.026

Highlights

- Showed the essential role of the effective geometric size of nanomaterials in studying nanoelasticity.
- Identified the proper definition for effective diameter / thickness for nanowire and nanofilms.
- Developed a simple model to explain the softening effect of surface bond loss on GaN nanowires.
- Performed molecular static simulations to quantify the effect of the surface bond loss on GaN nanowires

Effective Geometric Size and Bond-Loss Effect in Nano-elasticity of GaN Nanowires

R.J. Wang, C.Y. Wang*, Y.T. Feng

Zienkiewicz Centre for Computational Engineering, College of Engineering, Swansea University, Bay Campus, Swansea, SA1 8EN, UK

Keyword: GaN Nanowires, Surface elasticity, Size-dependence, Bond-loss effect, Effective size

Abstract This paper aims to identify a well-defined effective diameter of Nanowires (NWs) in evaluating their Young's modulus and to investigate the physical mechanisms behind the achieved surface elasticity. To this end, GaN NWs were considered for which a layer-wise model was developed and the tensile tests were performed based on molecular statics simulations (MSS). It was shown that two previously defined effective diameters result in an opposing effect of the surface elasticity and reversed size-dependence of the overall Young's modulus. Subsequently, a proper effective diameter was decided for the NWs, which enables one to correctly interpret atomistic simulations in terms of continuum mechanics concepts. In particular, clear evidence was attained showing that the bond loss on the NW surface results in around 43% surface softening relative to the NW interior and bulk material.

Corresponding author: chengyuan.wang@swansea.ac.uk

1. Introduction

Elasticity at the nanoscale [1–4] has garnered diverse interests in the past decades following successful synthesis of nanowire and nanofilm structures. Research efforts have mainly focused on characterizing the distinguishing effect of surfaces [5–14] to understand and reliably exploit the size-dependent overall elasticity of nanowires (NWs) and nanofilms (NFs) for next-generation applications. In the majority of studies [1–14], continuum elastic quantities (Young's modulus) defined for bulk materials has been directly adopted to assess the properties of nanomaterials.

In doing this, an issue known as 'Yakobson's paradox' [15-17] emerged in the effort of defining the effective thickness of carbon nanotubes (CNTs) to calculate their Young's modulus and bending stiffness. As reviewed in [17], extensive studies were carried out to resolve the issue and establish a well-defined thickness for CNTs. This effort is worthwhile as the effective geometric size of nanostructures is a key parameter that strongly influences the continuum mechanics analysis of and consequent understandings drawn from the atomistic calculations and nanoscale experimental data. Despite different effective diameters (thicknesses) defined for NWs (NFs) in previous computational studies, its impact on the corresponding elasticity characterisations has yet to be examined [4,18,19]. Considering the characteristic size range of size-dependent elasticity is below 20 nm, substantial uncertainties may exist in the surface elastic property and size dependence of NW elasticity obtained through various diameter definitions regardless of modelling techniques. Therefore, it is necessary and beneficial to pursue this issue in detail for NWs.

Concurrently, an array of studies was undertaken to elucidate the physical mechanisms underlying surface elastic property changes (softer or stiffer versus bulk) in NWs (/NFs). Based

on molecular statics (MS) and *ab-inito* calculation, Huang *et. al.* [20–22] demonstrated that the bulk deviating surface elasticity is a product of the competition between the surface coordination reduction or bond loss and the accompanying electron redistribution dependent surface relaxation or bond saturation. As the electronic structure is absent in empirical potential based studies, bond saturation can be broadly understood in terms of the resultant relaxation incited bond contraction strengthening as posited by Sun *et. al.* [23]. In particular, Agrawal and Bernal *et al.* [4,24] carried out a comprehensive study of semiconducting NWs via combined experiment and molecular dynamics simulations (MDS), and identified a correlation between the observed surface stiffening and the interatomic distance (*d*) contraction via the relation $Y \propto d^{-4}$ (Y: Young's modulus). On the other hand, bond loss is assumed to inflict elastic softening. Huang *et. al.* [20] estimated for Cu surface structures roughly 10%-25% stiffness reduction from bulk due to the bond loss. MDS of GaN nanostructures performed by Wang *et al.* [18,25] found, in agreement with experiments [26], softening of GaN NWs citing bond loss and weaker atomic cohesion at the surface. For NWs the bond loss effect remains to be quantified and its means of influencing elastic behaviour needs to be clarified. This provides impetus to carry out a detailed study of the bond loss effect on the surface elasticity of GaN NWs.

In the present paper, we carried out molecular statics calculations with Stillinger-Weber and Tersoff-Brenner semi-empirical potentials to examine the surface elastic behaviour of GaN NWs. Focus is placed on forming an appropriate effective diameter definition for accurate characterisation of NW surface elasticity in the size range where size-dependence manifests, and on investigating the physical mechanisms exhibited by the current models. The virtual tensile test procedure and a layer-wise model for GaN NWs are explained in Sec.2. The results and analysis are presented in Sec. 3, where the process to determine the effective geometric size and the

examination of the surface bond loss on the elasticity of GaN NWs are detailed. Conclusions are drawn in Sec.4.

2. Methodology

The following subsections detail the molecular statics (MS) tension procedure and the layer-wise modelling of GaN NWs. In particular, the latter is necessary for the quantitative profiling of the elastic property variations within the NW (especially on the surface), and provides insights into the impact of effective size measurements on the continuum mechanics based NW elasticity characterization.

2.1 Uniaxial tension modelling procedure

The elastic responses of GaN NWs were modelled via MS techniques utilizing the LAMMPS software package [27]. Following past MDS of GaN NWs and tubes [4,18,25,28] the Stillinger-Weber potential (SWp) was initially employed to describe interaction energies [29,30]. The specific form follows:

$$E = \sum_{i}\sum_{j>i} \varphi_2\,(r_{ij}) + \sum_{i}\sum_{j\neq i}\sum_{k>j} \varphi_3\,(r_{ij}, r_{ik}, \theta_{ijk})$$

$$\varphi_2\,(r_{ij}) = A_{ij}\,\varepsilon_{ij}\left[B_{ij}\left(\frac{\sigma_{ij}}{r_{ij}}\right)^{p} - \left(\frac{\sigma_{ij}}{r_{ij}}\right)^{q}\right]\exp\left(\frac{\sigma_{ij}}{r_{ij} - \alpha_{ij}\,\sigma_{ij}}\right)$$

$$\varphi_3\,(r_{ij}, r_{ik}, \theta_{ijk}) = \lambda_{ijk}\varepsilon_{ijk}\left[\cos\theta_{ijk} - \cos\theta_{0ijk}\right]^2 \exp\left(\frac{\gamma_{ij}\,\sigma_{ij}}{r_{ij} - \alpha_{ij}\,\sigma_{ij}}\right)\exp\left(\frac{\gamma_{ik}\,\sigma_{ik}}{r_{ik} - \alpha_{ik}\,\sigma_{ik}}\right)$$

The total energy E of a system of atoms consists of two-body φ_2 and three-body φ_3 angular contributions. r_{ij} is the relative distance between atoms i-j and θ_{ijk} is the angle between r_i and r_k subtended at the atom j as vertex. θ_{0ijk} is set to be the ideal tetrahedral angle to energetically favour the bulk wurtzite structure. ε_{ij} is the minimum pairwise interaction energy between atoms

i-j and $\alpha\sigma$ represents the cut-off distance. Other terms A, B, p, q, λ and γ are dimensionless fitting parameters to reproduce material properties. However, due to its formalism derived mostly under bulk assumptions, the SWp may not be able to reflect behavioral changes on surfaces [31]. Thus, the bond-order based Tersoff-Brenner potential (TFp), better suited for poorly coordinated surface environments, was also employed for comparisons and assessment of transferability [32,33]. The detailed form follows:

$$E = \sum_i \sum_{j>i} [\phi_{ij}(r_{ij}) - \bar{B}_{ij} \cdot \psi_{ij}(r_{ij})]$$

$$\bar{B}_{ij} = \frac{\sqrt{1+\chi_{ij}} + \sqrt{1+\chi_{jI}}}{2}$$

$$\chi_{ij} = \sum_{k \neq i,j} f_{ik}(r_{ik}) \cdot g_{ik}(\theta_{ijk}) \exp\left(2\mu_{ik}\left(r_{ij} - r_{ik}\right)\right)$$

$$\phi_{ij}(r_{ij}) = f_{ij}(r_{ij}) \cdot V_{ij}^{R}(r_{ij});\ \psi_{ij}(r_{ij}) = f_{ij}(r_{ij}) \cdot V_{ij}^{A}(r_{ij})$$

$$f_{ij}(r_{ij}) = f(x) = \begin{cases} 1, & r_{ij} \leq R_{ij} - D_{ij} \\ \frac{1}{2} - \frac{1}{2}\sin\left[\frac{\pi(r_{ij} - R_{ij})}{2D_{ij}}\right], & R_{ij} - D_{ij} < r_{ij} \leq R_{ij} + D_{ij} \\ 0, & r_{ij} > R_{ij} + D_{ij} \end{cases}$$

Here the total energy E is characterised by three functions ϕ_{ij}, ψ_{ij} and $\bar{B}_{ij}$ respectively representing the i-j repulsion, the i-j attraction and the bond order term. Specifically, B_{ij} accounts for the impact of local bonding environment on pairwise attractive energy through the local angular-dependent variable χ_{ij}. f_{ij} is a sinusoidal cutoff function, where $r_s = R - D$ is the cut-off starting radius and $r_c = R + D$ the distance where interaction energy vanishes. Both potentials were parameterized via lattice parameters, elastic constants and defect properties based on first principle and/or experimental measurements. The fitting parameter values for the SWp and the TFp can be found respectively in [30] and [33]. The fidelity of the SWp has been verified in the MD study of extended defects in GaN and the TFp based on accurate growth phase prediction for GaN vapor deposition.

As a prototypical case, this work considers hexagonal wurtzite GaN NWs with axis parallel to the [0001] crystallographic direction. The lateral facets comprise the nonpolar $\{10\bar{1}0\}$ planes. To assess the size dependence of Young's modulus in the [0001] direction, NWs of diameters 5 nm to 20 nm were subjected to tension in the axial direction. As a convention further usage of Young's modulus refers to Young's modulus in the [0001] direction unless stated otherwise. The NW length is set at five times the diameter for all cases and the periodic boundary condition was imposed along the loading direction to eliminate end effects.

The tensile test procedure was adopted from the method outlined by Huang *et al.* [1,20]. First, the energy-minimized structure of the NW was found by the conjugate gradient method and the corresponding total energy E for the NW and its component layers are computed by summing energies of the constituent atoms. The atoms consisting a component layer are those encompassed within its representative geometry as defined in section 2.2. Then displacement loading was applied at increments of 0.05% and up to a total engineering strain of 2% (smaller strain increments produced similar results). After each loading, the NW was again relaxed to a local energetic minimum with the conjugate gradient method and the total energy computations for the NW and its component layers were repeated.

2.2 Layer-wise NW model

To facilitate a similar layer-wise characterization of elasticity as [24] for GaN NWs, each NW was treated as an assembly of component atomic layers. Accordingly, by representing each layer (Fig.1(a)) with a continuous hexagonal cross-sectioned shell or prism, the equivalent volume of the layer (and total NW volume) can be estimated to enable Young's modulus evaluation. The geometry definition for each layer is as follows. Examining the NW cross

section (in Fig.1 (b) layers are selectively illustrated), the core or layer 1 consists of the six central atoms. Its hexagonal contour is then specified by connecting the six interstitial sites around the atoms. Extruding this contour along the NW length forms the hexagonal prism representing the first layer. The diameter of this prism ($d = 2t_1$) is then twice the distance between the diagonal interstitial sites leading to a cross-sectional area of $\frac{3\sqrt{3}}{2}t_1^2$. Ensuing layers are homogenized as hexagonal shells (Fig.1 (a)). For the *n*-th layer (*n* = 2, 3…, *N*-1) diameter d_n is defined as the diagonal length $2R_n$, for instance in Fig.1(c) $d_3 = 2R_3$. These layers exhibit a constant thickness defined as $t_n = R_n - R_{n-1}$, (t_3 is illustrated in Fig.1 (c)). The area of the *n*-th layer is thus equal to $\frac{3\sqrt{3}\left(R_n^2 - R_{n-1}^2\right)}{2}$.

Crucially, due to the boundary ambiguity at the outmost or surface layer, its effective thickness t_s (i.e. t_N) is captured by two limiting schemes: 1) the same definition as layers 2 to *N*-1 giving t_s of Fig.1 (d). This set an upper bound D_{up} for the NW diameter definition with an effective cross sectional area of $\frac{3\sqrt{3}}{8}D_{up}^2$. D_{up} was used to estimate the NW diameter in [18]. 2) Use the surface layer central line as the outer boundary of the associated hexagonal shell resulting in a thickness of $\frac{t_s}{2}$ (Fig.1 (e)). Accordingly, this establishes the lower bound D_{low} for the NW diameter and the cross sectional area is $\frac{3\sqrt{3}}{8}D_{low}^2$. We note that D_{low} is the adopted scheme in [4]. Finally, a continuous GaN NW body is formed by assembling individual layers with a continuous interface where identical stresses/strains and displacements are assumed between adjacent layers (or two neighbouring hexagonal prisms).

3. Results and discussion

With the above methodology, the surface effect was examined for GaN NWs of varying sizes. Emphasis is placed on the reduction of uncertainty in effective size determination for accurate elasticity size-dependence profiling and clarification of physical mechanisms exhibited.

3.1 Determination on the effective geometric size of NWs

The total energy of the entire NW and each component layer is first plotted against the axial strain, ε, and the total energy-axial strain function, E_{total}, then is found via polynomial fitting. The equivalent axial Young's modulus, *Y*, is computed for the NW and its constituent layers by taking the second derivative of E_{total} with respect to ε.

$$Y = \frac{1}{V_o}\left(\frac{\partial^2 E_{total}}{\partial \varepsilon^2}\right)_{\varepsilon=0} \quad (1)$$

Here V_o is the volume of the unloaded NW structure or component layers. Based on SWp and TFp, the axial Young's modulus of an NW (Y_{NW}) was calculated for NWs of different sizes. The overall Y_{NW} obtained under D_{up} and D_{low} (used in V_o evaluation) are presented in Fig.2. It is interesting to see that no matter which interaction potential is used, D_{low} always leads to increasing Y_{NW} with decreasing diameter, whereas D_{up} gives the opposite size-dependence where Y_{NW} declines as the diameter decreases. In particular, the size-dependence associated with D_{low} agrees with the study by Bernal *et al.* [4] and the results from D_{up} are consistent with

the findings by Wang *et al.* [25]. Thus, the present simulations are reliable, which indicates that the choice of the effective diameter is critical in predicting the size-dependence of Y_{NW} for discrete NWs.

To understand the divergence caused by D_{low} and D_{up} in Fig.2, the radial Young's modulus distribution was constructed by calculating the axial Young's modulus for individual layers, Y_l , of the NW using the SWp generated total energy data (TFp gives similar results). The radial distributions of Y_l / Y_{bulk} are shown in Fig.3, where Y_{bulk} is the bulk value. As evident for all NW sizes, the Young's modulus of the outmost layer Y_l^s is 50% higher than Y_{bulk} when D_{low} or the effective surface thickness $\frac{t_s}{2}$ is assumed. On the contrary, Y_l^s becomes 25% lower than Y_{bulk} when D_{up} or the effective surface thickness t_s is used. All layers in the interior, however, hold Y_l equal to or slightly above Y_{bulk}. Consequently, the sense of Y_{NW} deviation from Y_{bulk} is controlled by Y_l^s which scales with the effective surface thickness, i.e. D_{low} leads to $Y_l^s > Y_{bulk}$ and accordingly $Y_{NW} > Y_{bulk}$, whereas D_{up} yields $Y_l^s < Y_{bulk}$ and $Y_{NW} < Y_{bulk}$. Finally, as the atomic percentage of surface atoms rises with the NW size decreases (e.g., 6% for 20*nm* NW and 20% for 5*nm* NW) the contribution of surface Young's modulus Y_l^s to NW Young's modulus Y_{NW} increases and hence an opposing size-dependency of Y_{NW} manifests as in Fig.2.

Clearly, the wide discrepancy observed in Fig.2 stems from the ambiguous thickness measurement on the discretized surface layer. As reviewed before, the effective thickness (or size) of nanostructures has been studied extensively for single-atom layer CNTs [17] and single-protein layer microtubules [34]. However, so far, this issue has not been discussed for NWs,

which are an assembly of many atom layers and thus are tacitly assumed to be a continuous body. Nevertheless, as shown above, for small (< 20 nm) NWs with a high atomic percentage of surface atoms, effective size determination becomes crucial to correctly characterizing the overall elastic property and elucidating the underpinning mechanisms.

Consequently, current estimation schemes for the effective surface thickness or NW diameter need to be refined to resolve the response obfuscation observed in Fig.2. To this end, an equivalent axial elastic modulus (S_p) defined in Eq.2 is adopted for an NW and its component layers, independent of the definition of their effective volume:

$$S_p = \frac{\partial^2}{\partial \varepsilon^2}\left(\frac{E_{total}}{N_d}\right)_{\varepsilon=0} \tag{2}$$

As the stoichiometric ratio is maintained within each NW and its component layers, E_{total} in Eq.2 is normalized with N_d, the number of Ga-N dimer or formula unit (f.u.), instead of V_o, to give the average energy per f.u. (E_p) of an NW or its individual layers.

The calculated radial distributions of S_p and E_p are presented for all NWs in Fig.4 (SWp) and Fig.5 (TFp). Evident from Figs.4a and 5a, the surface elastic modulus declined by ~25% versus the constant bulk values held by the interior. This surface modulus modification quantitatively matches the surface Young's modulus reduction present in Fig.3 (a) based on D_{up} and disagrees with the surface Young's modulus rise predicted in Fig.3 (b) using D_{low} . The radial distribution of stored strain energy per f.u. in Figs. 4b and 5b further corroborates this behavior, as the absolute strain energy absorption is minimal on the outmost atom layer. The coherence with D_{up} results identifies the upper bound diameter and the effective surface thickness *t* as the more appropriate choice for evaluating the effect of surface elasticity and the size-dependence of Young's modulus of an NW. This is simply because between the surface

layer and an inner layer, the volume ratio is equal to the atom number ratio when the surface thickness t is assumed. On the other hand, the previously used D_{low} is likely biased and thus should be avoided in the future study of the elasticity of thin NWs.

As shown above, the definition of effective size or thickness is essential for the study of nanostructures as it serves as a linkage between atomistic simulations and equivalent continuum mechanics models. This is especially important for thin NWs where the effective diameter definition greatly impacts on the equivalent Young's modulus valuation at the surface layer and through it on the change of NW Young's modulus from the bulk.

3.2 Physical mechanisms of surface effect

In past studies of nano-elasticity the combined effects of surface bond loss and resulting surface relaxation incited bond contraction were purposed to elucidate the divergence of surface elastic behavior from the bulk material [1,4,20]. For GaN NWs, bond contraction was indeed observed in structural studies based on density functional theory (DFT) [35,36], which may yield elastic stiffening via the relation $Y \propto d^{-4}$ [4,37]. Bond loss is generally considered to be responsible for elastic softening but the extent and specific mechanisms of its influence on the surface elasticity has not been detailed for GaN NWs.

To address these issues, we examined the initial energy minimized NW structure found via both the SWp and the TFp to characterise the surface relaxation in terms of local and overall structural alterations. Under the SWp, no variation from the bulk bond geometry was produced on the surface and the layer structures do not sustain any residual axial strain. In the TFp simulation, the minimized structure showed 1-1.2% contraction of the Ga-N back bond on the surface and 0.6-1.5% contraction of the axial bond (Fig. 6a). The former is relatively closer to

the DFT benchmark (2%) whereas the latter (more important for axial elastic modulus) is much lower than the 7% found by the DFT [35,36]. This generates 1.6% axial compressive strain on the surface layer and corresponding tensile strains of 0.27-0.59% on the interior layers. The employed TFp offers improvements but, obviously, still cannot well reproduce the $\{10\bar{1}0\}$ surface relaxation. Thus, the surface softening seen in TFp (Fig. 5) and SWp (Fig. 4) should dominantly reflect the action of the bond loss mechanism [20].

This elastic softening of the GaN surface layer in the [0001] direction can be understood through a simplified account of the structural effect due to surface coordination reduction. A bulk Ga-N pair aligned to the [0001] direction and its nearest neighbors can be considered as a tetrahedrally braced structural element (Fig. 6b). On $\{10\bar{1}0\}$ surfaces, the coordination number is reduced to three. Two bonds or braces that are not perpendicular to the loading direction are lost, and consequently, the structural elements on surfaces become poorly reinforced against a [0001] directed strain. As a result, the constraints imposed on the surface atomic chains is less than in the core of the NW. From the point of view of continuum mechanics, this leaves the surface layer in plane stress state while the interior region of NWs is in the three dimensional stress state. The surface layer therefore becomes more compliant compared to the interior layers. As such, the equivalent elastic modulus S_p of the outmost layer should be lower than the interior layers to reflect such a decline in structural rigidity.

For quantitative confirmation, the outmost layer structure of the NW is further divided, based on coordination number, into two sub-layers for which the S_p is calculated respectively. From Fig. 6c, the outer sub-layer consists of all under-coordinated atoms (with bond loss) while the inner sub-layer contains the fully coordinated atoms (no bond loss). To account for different bulk values given by the potentials, S_p in Table 1 is normalized by the bulk value for all layers of

the 5 nm NW. By both potentials, the S_p of under-coordinated atoms (the outer sub-layer) is ~43% lower than the bulk; while the S_p of the fully coordinated atoms (the inner sub-layer) holds less than 3% difference from the bulk S_p. This calculation provides direct evidence that the surface softening achieved in the simulations is indeed a result of the bond loss on the outmost layer of the NWs. In particular, the 43% reduction of S_p in the outer sub-layer of the outmost layer (Table 1) or the 25% reduction achieved for the whole outmost layer (Figs.4a and 5a) based on the SWp and the TFp can be considered as a quantitative measurement on the direct impact of the bond loss.

In addition, the TFp reported a normalised S_p of 1.019 for the inner sub-layer – with an increase of 4.3% over the 0.976 given by the SWp – showing a detectable stiffening effect of bond contraction. However, with similar magnitude of bond contraction across the surface layer (unlike DFT predictions [35,36]) potential stiffening effect on the outer sub-layer of remains minor. Specifically, the contribution of bond contraction to surface elasticity should remain around an order of magnitude lesser than the impact of the bond loss, and thus, negligible in overall surface elasticity shown in the TFp results (Fig. 5).

As shown above, DFT predicted greater surface relaxation and hence increased amount of surface elasticity stiffening. Therefore, the resultant surface effect obtained by the TFp here will deviate from the accurate value for GaN NW. Adequate capture of poorly coordinated states by an empirical potential remains an eminent challenge in further understanding of GaN NW surface effect and size-dependence at the current scale. The difficulty is rooted in the mixed ionic-covalent nature of Ga-N bonds and variation of bonding nature with the electron redistribution. The modified Tersoff potential incorporating ionicity based long-range interactions and a simple core-shell potential may offer a possible solution [38,39].

4. Conclusion

A layer-wise model developed for GaN NWs and the MS technique were employed to examine the role of the effective diameter in studying the surface elasticity and the size-dependence of overall elasticity for the NWs. Subsequently, the physical mechanisms behind the surface softening were discussed and the bond loss effect was evaluated based on the SWp and the TFp. The conclusions drawn in the present study are as follows.

The effective diameter plays an important role in studying the elasticity of thin GaN NWs (diameter smaller than 20 nm) as it alters the effective thickness of the outmost atom-layer and thus, the value of surface Young's modulus. Different effective diameters are shown to inflict substantial divergence or even the opposite size-dependence of overall Young's modulus. Herein, the upper bound diameter in Sec.2.2 is found to be well-defined and is able to consistently reflect the surface elasticity and the size-dependent Young's modulus of GaN NWs.

The bond loss on the surface layers is found to be responsible for surface softening achieved in the present MS simulations relative to the corresponding bulk. This arises from the reduction of constrains on surface atoms as compared to the NW core. As a result, the surface layer is more compliant when subjected to an axial deformation. Specifically, the decrease of the surface elasticity due to the bond loss is measured to be around 43% for GaN NWs.

In addition, it should be pointed out that the net surface effect on GaN NWs includes both the bond loss and the bond contractions. Its proper determination and confirmation still awaits the development of an empirical potential that can appropriately describe the various poorly coordinated states of the materials system.

References

[1] Liang H, Upmanyu M, Huang H. Size-dependent elasticity of nanowires: Nonlinear effects. Phys Rev B - Condens Matter Mater Phys 2005;71:1–4.

[2] Lee C, Wei X, Kysar JW, Hone J. Measurement of the elastic properties and intrinsic strength of monolayer graphene - Supplementary Information. Science 2008;321:385–8.

[3] Hernández E, Goze C, Bernier P, Rubio A. Elastic properties of C and BxCyNz composite nanotubes. Phys Rev Lett 1998;80:4502–5.

[4] Bernal RA, Agrawal R, Peng B, Bertness KA, Sanford NA, Davydov A V., et al. Effect of growth orientation and diameter on the elasticity of GaN nanowires. A combined in situ TEM and atomistic modeling investigation. Nano Lett 2011;11:548–55.

[5] Miller RE, Shenoy VB. Size-dependent elastic properties of nanosized structural elements. Nanotechnology 2000;11:139–47.

[6] Diao J, Gall K, L. Dunn M. Atomistic simulation of the structure and elastic properties of gold nanowires. J Mech Phys Solids 2004;52:1935–62.

[7] Dingreville R, Qu J, Mohammed Cherkaoui. Surface free energy and its effect on the elastic behavior of nano-sized particles, wires and films. J Mech Phys Solids 2005;53:1827–54.

[8] Chen C, Shi Y, Zhang Y, Zhu J, Yan Y. Size dependence of Young's modulus in ZnO nanowires. Phys Rev Lett 2006;96:75505.

[9] Diao J, Gall K, Dunn ML, Zimmerman JA. Atomistic simulations of the yielding of gold nanowires. Acta Mater 2006;54:643–53.

[10] Lucas M, Mai W, Yang R, Wang ZL, Riedo E. Aspect Ratio Dependence of the Elastic Properties of ZnO Nanobelts. Nano Lett 2007;7:1314–7.

[11] He M-R, Shi Y, Zhou W, Chen JW, Yan YJ, Zhu J. Diameter dependence of modulus in zinc oxide nanowires and the effect of loading mode: In situ experiments and universal core-shell approach. Appl Phys Lett 2009;95:91912.

[12] Xu F, Qin Q, Mishra A, Gu Y, Zhu Y. Mechanical properties of ZnO nanowires under different loading modes. Nano Res 2010;280:1–10.

[13] Sadeghian H, Goosen JFL, Bossche A, Thijsse BJ, van Keulen F. Effects of size and surface on the elasticity of silicon nanoplates: Molecular dynamics and semi-continuum approaches. Thin Solid Films 2011;520:391–9..

[14] Gong B, Chen Q, Wang D. Molecular dynamics study on size-dependent elastic properties of silicon nanoplates. Mater Lett 2012;67:165–8.

[15] Yakobson BI, Brabec CJ, Bernholc J. Nanomechanics of carbon tubes: Instabilities beyond linear response. Phys Rev Lett 1996;76:2511–4.

[16] Huang Y, Wu J, Hwang KC. Thickness of graphene and single-wall carbon nanotubes. Phys Rev B - Condens Matter Mater Phys 2006;74:5413.

[17] Wang CY, Zhang LC. A critical assessment of the elastic properties and effective wall thickness of single-walled carbon nanotubes. Nanotechnology 2008;19:75705.

[18] Wang Z, Zu X, Yang L, Gao F, Weber WJ. Orientation and temperature dependence of the tensile behavior of GaN nanowires: an atomistic study. J Mater Sci Mater Electron 2007;19:863–7.

[19] Agrawal R, Espinosa HD. Giant piezoelectric size effects in zinc oxide and gallium nitride nanowires. A first principles investigation. Nano Lett 2011;11:786–90.

[20] Zhou LG, Huang H. Are surfaces elastically softer or stiffer? Appl Phys Lett 2004;84:1940–2.

[21] Zhang L, Huang H. Young's moduli of ZnO nanoplates: Ab initio determinations. Appl Phys Lett 2006;89:9–12.

[22] Shim HW, Zhou LG, Huang H, Cale TS. Nanoplate elasticity under surface reconstruction. Appl Phys Lett 2005;86:1–3.

[23] Sun CQ. Oxidation electronics: Bond-band-barrier correlation and its applications. Prog Mater Sci 2003;48:521–685.

[24] Agrawal R, Peng B, Gdoutos EE, Espinosa HD. Elasticity size effects in ZnO nanowires-A combined experimental- computational approach. Nano Lett 2008;8:3668–74.

[25] Wang Z, Zu X, Gao F, Weber WJ. Mechanical behavior of gallium nitride nanotubes under combined tension-torsion: An atomistic simulation. J Appl Phys 2008;103:42–5.

[26] Nam C-Y, Jaroenapibal P, Tham D, Luzzi DE, Evoy S, Fischer JE. Diameter-dependent electromechanical properties of GaN nanowires. Nano Lett 2006;6:153–8.

[27] Plimpton S. Fast Parallel Algorithms for Short – Range Molecular Dynamics. J Comput Phys 1995;117:1–19.

[28] Xu B, Lu AJ, Pan BC, Yu QX. Atomic structures and mechanical properties of single-crystal GaN nanotubes. Phys Rev B - Condens Matter Mater Phys 2005;71:1–6.

[29] Stillinger FH, Weber TA. Computer simulation of local order in condensed phases of silicon. Phys Rev B 1985;31:5262–71.

[30] Béré A, Serra A. On the atomic structures, mobility and interactions of extended defects in GaN: dislocations, tilt and twin boundaries. Philos Mag 2006;86:2159–92.

[31] Zhou XW, Jones RE, Laboratories SN. Effects of Cutoff Functions of Tersoff Potentials

on Molecular Dynamics Simulations of Thermal Transport 2012:1–10.

[32] Tersoff J. New empirical approach for the structure and energy of covalent systems. Phys Rev B 1988;37:6991–7000.

[33] Nord J, Albe K, Erhart P, Nordlund K. Modelling of compound semiconductors: analytical bond-order potential for gallium, nitrogen and gallium nitride. J Phys Condens Matter 2003;15:5649–62.

[34] Wang CY, Ru CQ, Mioduchowski A. Orthotropic elastic shell model for buckling of microtubules. Phys Rev E - Stat Nonlinear, Soft Matter Phys 2006;74:2901.

[35] Carter DJ, Gale JD, Delley B, Stampfl C. Geometry and diameter dependence of the electronic and physical properties of GaN nanowires from first principles. Phys Rev B - Condens Matter Mater Phys 2008;77:5349.

[36] Wang Z, Wang S, Li J, Gao F, Weber WJ. Structure and Electronic Properties of Saturated and Unsaturated Gallium Nitride Nanotubes. J Phys Chem C 2009;113:19281–5.

[37] Agrawal R, Peng B, Gdoutos EE, Espinosa HD. Elasticity Size Effects in ZnO Nanowires−A Combined Experimental-Computational Approach. Nano Lett 2008;8:3668–74.

[38] Zapol P, Pandey R, Gale JD. An interatomic potential study of the properties of gallium nitride 1997;9:9517–25.

[39] Ito T, Akiyama T, Nakamura K. Systematic approach to developing empirical interatomic potentials for III – N semiconductors structural stability Systematic approach to developing empirical interatomic potentials for III – N semiconductors. Jpn J Appl Phys 2016;55:FM02.

[40] Stukowski A. Visualization and analysis of atomistic simulation data with OVITO–the

Open Visualization Tool. Model Simul Mater Sci Eng 2009;18:5012.

Tables

Normalized S_p	FCN	UCN	L_{s2}	Interior
Tersoff	1.019	0.564	1.0272	1
SW	0.976	0.576	1.0238	1

Table 1. Bulk value normalized elastic modulus (S_p) of the component layers and atom groups for the 5 nm nanowire. From left to right: the surface layer (L_s) separated into its fully coordinated (FCN) atom group and under-coordinated (UCN) atom group, the last interior layer (L_{s2}) and the average of all interior layers.

Figures

Figure 1. Nanowire and component layer effective thickness (or volume) estimation scheme

Figure 2. Overall NW Young's modulus calculated using SWp and TFp for the entire size range

Figure 3. Distribution of Effective Layer Young's Modulus or Young's Modulus Radial Distribution of each NW (SWp)

Figure 4. SWp based Strain Energy and S_p Radial Distribution

Figure 5. TFp based Strain Energy and S_p Radial Distribution

Figure 6. From left to right a) GaN bond types b) Coordination state of atoms in GaN NW (left) fully coordinated or bulk atom and (right) under coordinated or outermost surface atom c) Side view of the NW surface layer ($[1\bar{1}00]$ plane). Illustrates the division of the surface layer into under-coordinated (UCN) group (green) and fully-coordinated (FCN) group (orange)

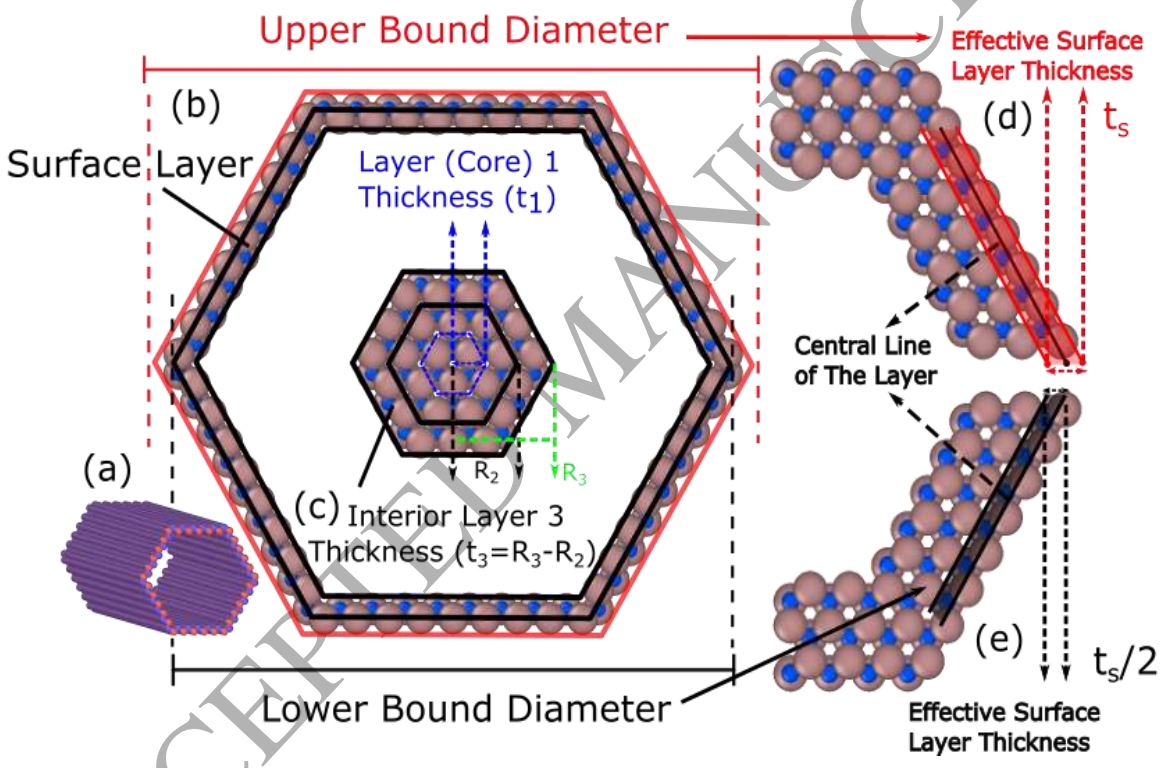

Figure 2. Nanowire and component layer effective thickness (or volume) estimation scheme [40]

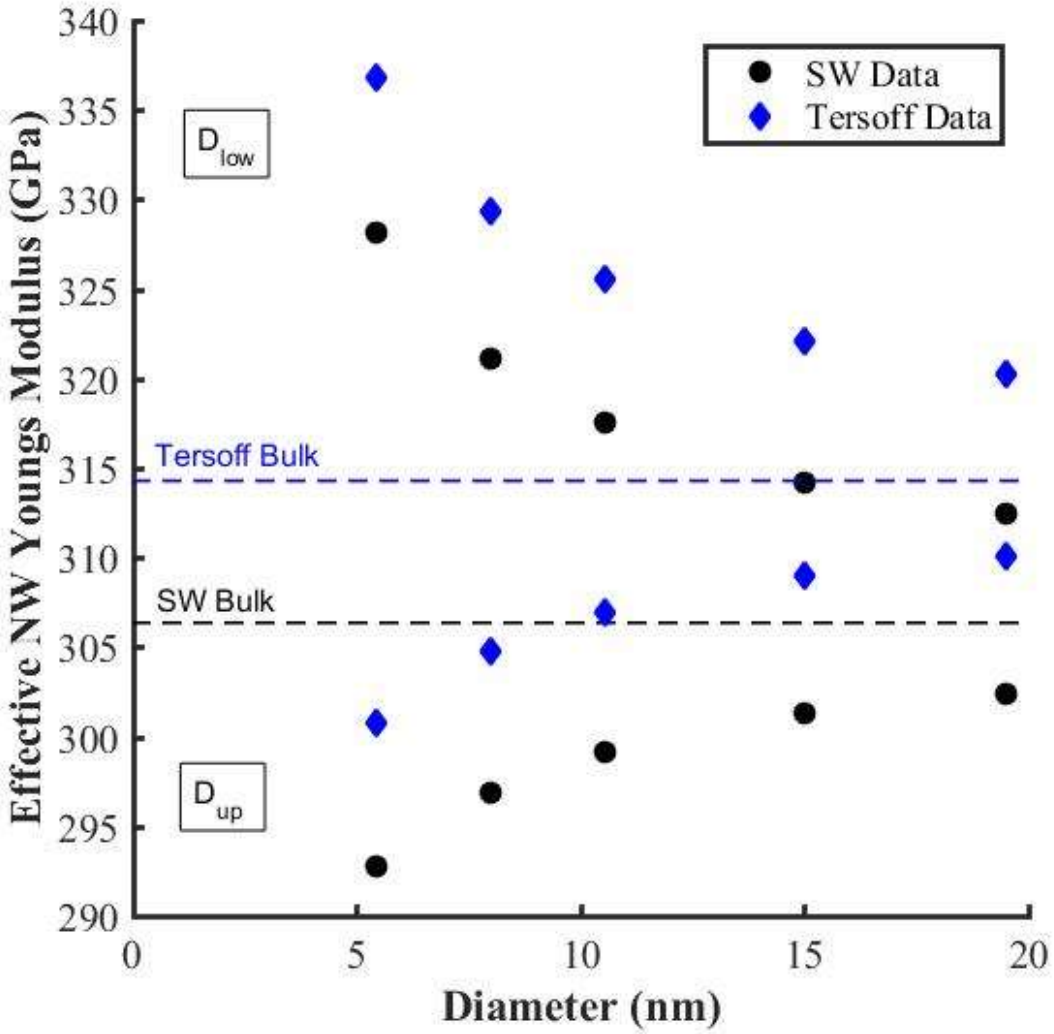
SW Data
Tersoff Data
D low
Tersoff Bulk
SW Bulk
D up
Effective NW Youngs Modulus (GPa)
Diameter (nm)
340
335
330
325
320
315
310
305
300
295
290
0
5
10
15
20

Figure 2. Overall NW Young's modulus calculated using SWp and TFp for the entire size range

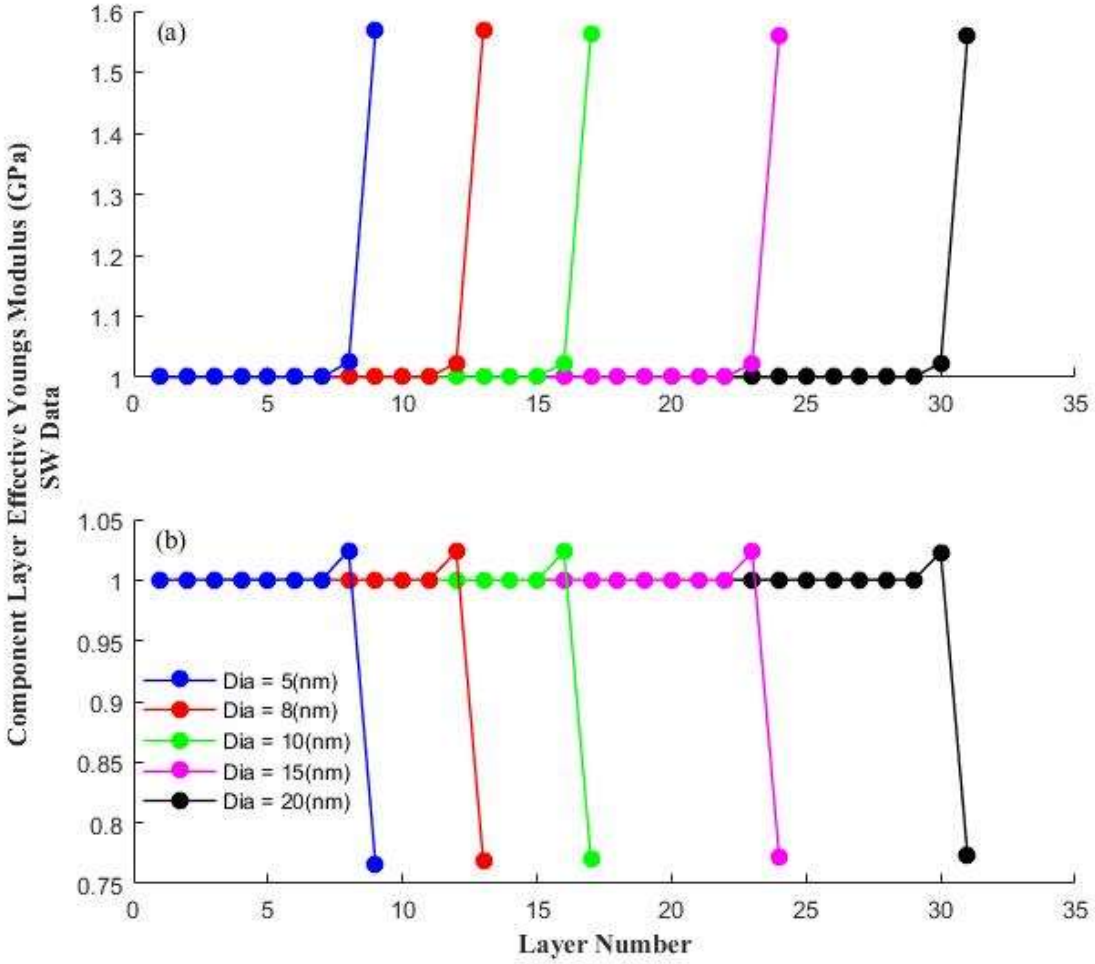

Figure 3. Distribution of Effective Layer Young's Modulus or Young's Modulus Radial Distribution of each NW (SWp)

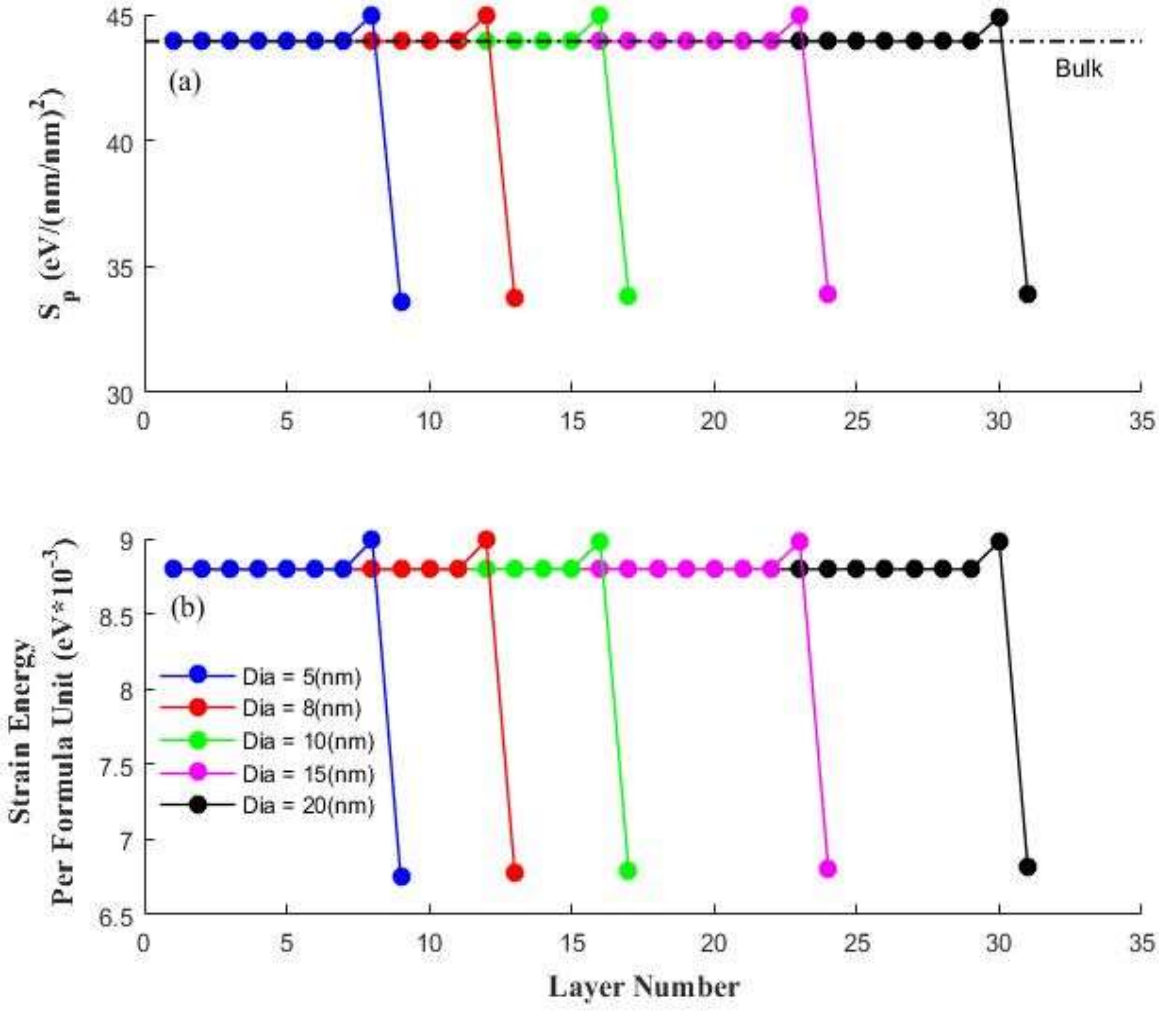

Figure 4. SWp based Strain Energy and S_p Radial Distribution

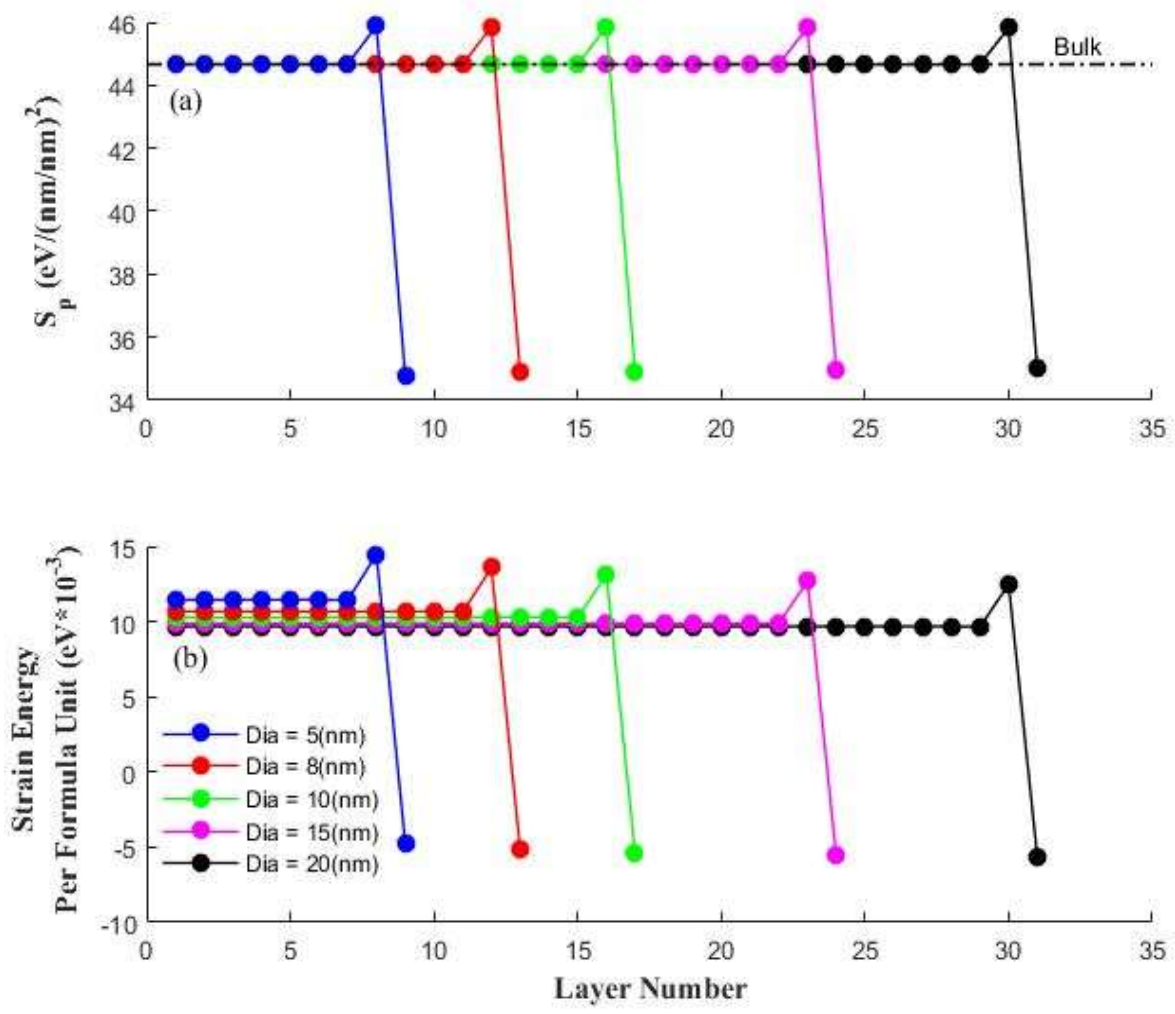

Figure 5. Tersoff based Strain Energy and S_p Radial Distribution

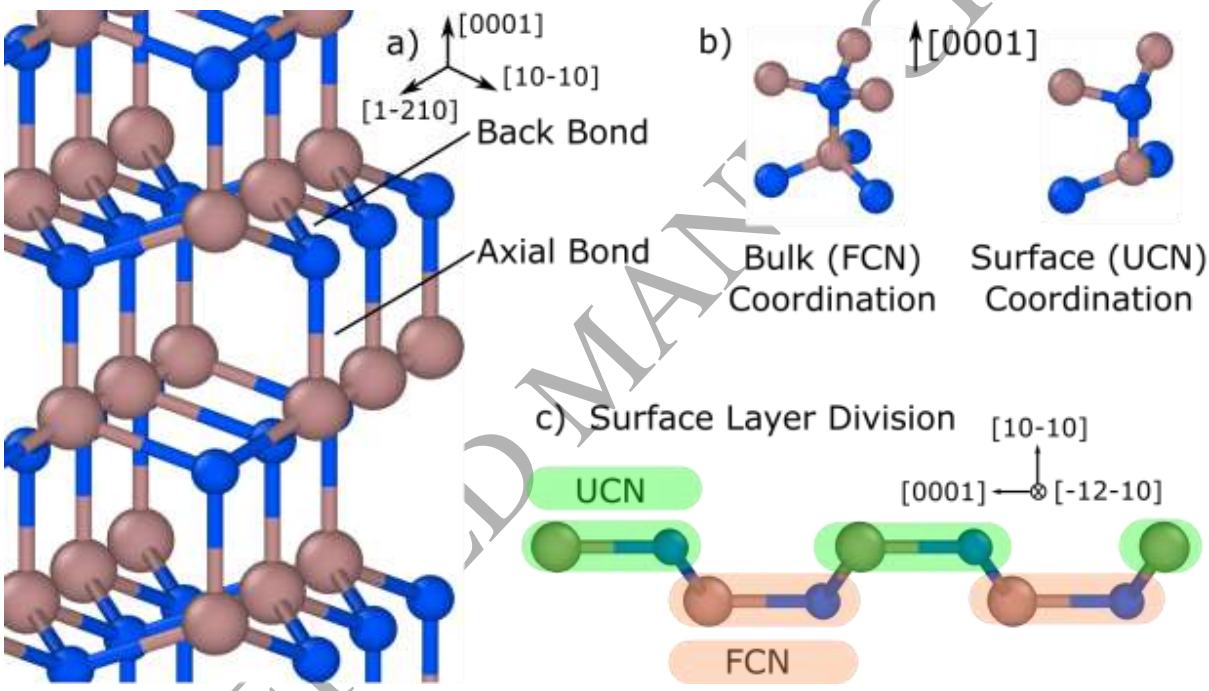

Figure 6. From left to right a) GaN bond types b) Coordination state of atoms in GaN NW (left) fully coordinated or bulk atom and (right) under coordinated or outermost surface atom c) Side view of the NW surface layer ($[10\bar{1}0]$ plane). Illustrates the division of the surface layer into under-coordinated (UCN) group (green) and fully-coordinated (FCN) group (orange) [40]

Graphical abstract